https://doi.org/10.5194/essd-2024-240
Preprint. Discussion started: 26 June 2024

Open Access Earth System Science Data Discussions

Coastal Atmosphere & Sea Time Series (CoASTS) and Bio-Optical mapping of Marine optical Properties (BiOMaP): the CoASTS-BiOMaP dataset.

Giuseppe Zibordi[1,2] and Jean-François Berthon[2]

[1]*National Aeronautics and Space Administration, Goddard Space Flight Center, MD USA*
[2]*Joint Research Centre of the European Commission, Ispra, Italy*

Correspondence to: Giuseppe Zibordi (giuseppe.zibordi@eoscience.eu)

https://doi.org/10.5194/essd-2024-240
Preprint. Discussion started: 26 June 2024

Open Access Earth System Science Data Discussions

ABSTRACT

The *Coastal Atmosphere & Sea Time Series* (CoASTS) and the *Bio-Optical mapping of Marine optical Properties* (BiOMaP) programs produced bio-optical data supporting satellite ocean color applications for almost two decades. Specifically, relying on the Acqua Alta Oceanographic Tower (AAOT) in the northern Adriatic Sea, from 1995 till 2016 CoASTS delivered time series of marine water apparent and inherent optical properties, in addition to the concentration of major optically significant water constituents. Almost concurrently, from 2000 till 2022 BiOMaP produced equivalent spatially distributed measurements across major European Seas. Both, CoASTS and BiOMaP applied equal standardized instruments, measurement methods, quality control schemes and processing codes to ensure temporal and spatial consistency to data products. This work presents the CoASTS and BiOMaP near surface data products, named CoASTS-BiOMaP, of relevance for ocean color bio-optical modelling and validation activities.

https://doi.org/10.5194/essd-2024-240
Preprint. Discussion started: 26 June 2024

Open Access Earth System Science Data Discussions

1. Introduction

The validation of primary (*i.e.,* radiometric) and derived (*e.g.,* phytoplankton pigments concentration) satellite data products, as well as the development of bio-optical algorithms linking radiometric data to the inherent optical properties or to the concentration of natural water optically significant constituents, require accurate and comprehensive *in situ* bio-optical measurements (*e.g.,* see Werdell and Bailey 2007). Anticipating this need for the Sea-Wide Field-of-View (SeaWiFS) ocean color mission, during the 90s several measurement programs were established to gather bio-optical data representative of the world marine waters. Among these, the *Coastal Atmosphere & Sea Time Series* (CoASTS) and the *Bio-Optical mapping of Marine optical Properties* (BiOMaP) measurement programs implemented by the Marine Optical Laboratory (Belward et al. 2022) of the Joint Research Center (JRC) in collaboration with a number of European institutions, produced comprehensive *in situ* bio-optical measurements of relevance for satellite ocean color applications. While CoASTS benefited of the Acqua Alta Oceanographic Tower (AAOT) in the northern Adriatic Sea to generate time-series data at a fixed coastal site (Berthon et al. 2002; Zibordi et al. 2002), BiOMaP relied on oceanographic ships to collect spatially distributed measurements across various European Seas (Berthon et al. 2008, Zibordi et al. 2011). Both CoASTS and BiOMaP endorsed standardization of instruments, measurement methods, quality control schemes and processing codes to enforce temporal and spatial consistency to data products.

Objective of this work is to introduce the CoASTS and BiOMaP derived data products relevant for satellite ocean color applications. Specifically, the near-surface data products, which constitute the CoASTS-BiOMaP data set, are presented together with a description of the measurement and data reduction methods.

2. The CoASTS and BiOMaP programs

CoASTS and BiOMaP were conceived as complementary programs: CoASTS focused on the generation of time-series of reference data from a single coastal site exhibiting significant seasonal cycles and moderately bio-optical complexity (Berthon et al. 2002); conversely BiOMaP covered a variety of marine regions exhibiting very diverse bio-optical regimes, but with limited temporal representativity (Berthon et al. 2008).

The use of an oceanographic tower as logistic platform for comprehensive optical and bio-geochemical measurements, when compared to oceanographic ships, does not allow for spatially extended observations. However, it offers the unique opportunity of a very stable measurement platform enabling easy control of the deployment geometry of optical instruments with respect to the structure. Specifically, regardless of sea state, the use of the AAOT as measurement platform made possible deploying optical sensors relying on tower–sensor–Sun geometry favouring the application of corrections for the minimization of potential superstructure perturbations in radiometric data (Zibordi et al. 1999, Doyle and Zibordi 2002).

CoASTS measurements are representative of marine frontal regions exhibiting occurrence of both Case 1 (*i.e.,* with optical properties of water largely determined by phytoplankton and degradation) and moderately optically complex waters characterized by modest concentrations of sediments and coloured organic matter (CDOM), with bio-optical variability determined by the impact of local currents, seasonal changes in biological regimes and rivers discharge (Berthon et al. 2002).

CoASTS measurements took place with monthly occurrence since 1995. However, from 2001 and up to the end of the measurement program in 2016, the frequency of field

https://doi.org/10.5194/essd-2024-240
Preprint. Discussion started: 26 June 2024

Open Access Earth System Science Data Discussions

measurements was reduced to one every 2-3 months. Each comprehensive data collection — called a *station* — included in-water optical and hydrographic profiles, seawater samples at different depths (*i.e.*, near surface, 8 m and 14 m), meteorological data, and visual observations of cloud cover and sea state. CoASTS comprises 176 field campaigns leading to 883 measurement stations. Still, only CoASTS campaigns and stations performed from December 1998 onward (*i.e.*, 125 and 617, respectively) fulfil standardization of measurements.

Comprehensive and spatially distributed measurements are best possible using oceanographic ships. Because of this, BiOMaP measurements were performed relying on research vessels across a variety of marine regions representing very diverse bio-optical features (see Berthon et al.2008): the Baltic Sea exhibiting waters dominated by a high concentration of CDOM; the Adriatic Sea, Black Sea, North Sea (including the English Channel), Ligurian Sea, Iberian Shelf and the Greenland Sea, characterized by a variety of optically complex waters determined by diverse concentrations of CDOM and total suspended matter (TSM); the Eastern and Western Mediterranean oligotrophic and mesotrophic Seas largely characterized by Case 1 waters.

BiOMaP, encompassing 36 bio-optical oceanographic campaigns and 1915 measurement stations, started in 2000 and ended in 2022. As already anticipated, measurement consistency between the CoASTS and BiOMaP programs was achieved using identical field and laboratory instrumentation, and attempting the application of the same consolidated measurement methods, quality control schemes and processing codes. Consequently, BiOMaP measurements performed during each station have correspondence with those of CoASTS, except for restricting the collection of water samples to the near surface. Additionally, superstructure perturbations in BioMaP radiometric data were avoided by operating optical radiometers on free-fall profilers deployed at some distance from ships.

Figure 1 shows the temporal evolution of CoASTS campaigns and the number of stations per campaign. These latter were mostly driven by the meteorological conditions which may have prevented access to the tower. Figure 2 shows the overall distribution of BiOMaP stations across the various European Seas.

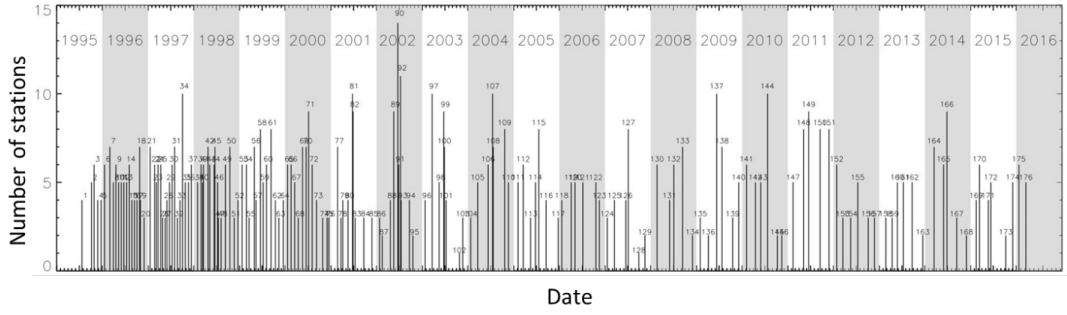

Figure 1. CoASTS measurement campaigns (176 total, 125 since December 1998) and stations (883 total, 617 since December 1998) completed between 1995 and 2016.

https://doi.org/10.5194/essd-2024-240
Preprint. Discussion started: 26 June 2024

Open Access Earth System Science Data Discussions

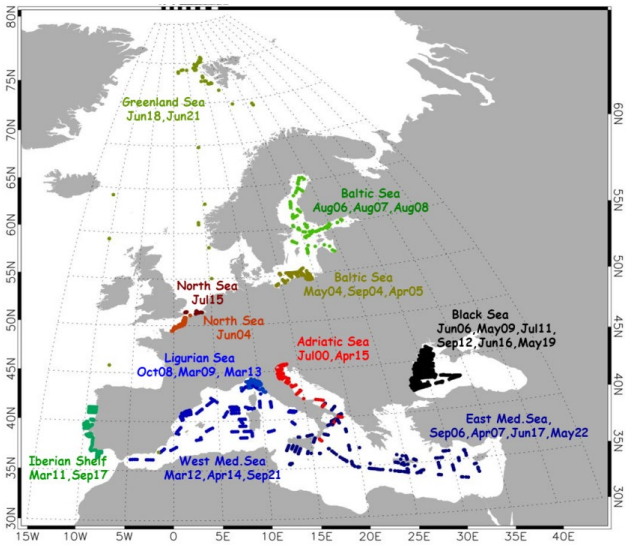

Figure 2. BiOMaP oceanographic campaigns (36) and measurement stations (1915) performed between 2000 and 2022.

Table 1. The CoASTS measurement program: campaign identifiers, marine region, years, number of stations, research platform, collaborating institution.

Campaign ID	Location	Year	Stations #	Research platform	Collaborating Institution
V03-V99	Northern Adriatic Sea (AAOT)	1998-2011	481	*Acqua Alta Oceanog. Tower (AAOT)*	Italian National Research Council (IT)
W01-W28	Northern Adriatic Sea (AAOT)	2011-2016	136	*Acqua Alta Oceanog. Tower (AAOT)*	Italian National Research Council (IT)

Table 2. The BiOMaP measurement program: campaign identifiers, marine regions, year, number of stations, research vessels, collaborating institutions.

Campaign ID	Region	Year	Stations #	Research vessel	Collaborating Institution
A01	Adriatic Sea (ADRS)	2000	55	*R/V Friuli-Venezia Giulia (FVG)*	University of Trieste (IT)
A02	Adriatic Sea (ADRS)	2014	66	*R/V Minerva-1*	Italian National Research Council (IT)
B01	Baltic Sea (BLTS)	2004	52	*R/V Oceania*	Institute of Oceanology (PL)
B02	Baltic Sea (BLTS)	2004	52	*R/V Oceania*	Institute of Oceanology (PL)
B03	Baltic Sea (BLTS)	2005	63	*R/V Oceania*	Institute of Oceanology (PL)
B04	Baltic Sea (BLTS)	2006	23	*R/V Aranda*	Institute of Marine Research (FL)
B05	Baltic Sea	2007	38	*R/V Aranda*	Institute of Marine Research

https://doi.org/10.5194/essd-2024-240
Preprint. Discussion started: 26 June 2024

	(BLTS)				(FL)
B06	Baltic Sea (BLTS)	2008	47	*R/V Aranda*	Institute of Marine Research (FL)
E01	Eastern Med. Sea (EMED)	2006	62	*R/V Urania*	Italian National Research Council (IT)
E02	Eastern Med. Sea (EMED)	2007	69	*R/V Urania*	Italian National Research Council (IT)
E03	Eastern Med. Sea (EMED)	2017	51	*R/V Minerva-1*	Italian National Research Council (IT)
E04	Eastern Med. Sea (EMED)	2022	31	*R/V Philia*	Hellenic Centre for Marine Research (GR)
I01	Iberian Shelf (IBSH)	2011	68	*NRP Almirante Gago Coutinho*	Portuguese Hydrographic Institute (PT)
I02	Iberian Shelf (IBSH)	2017	62	*NRP Almirante Gago Coutinho*	Portuguese Hydrographic Institute (PT)
K01	Black Sea (BLKS)	2006	93	*R/V Akademik*	Institute of Oceanology (BG)
K02	Black Sea (BLKS)	2009	73	*R/V Akademik*	Institute of Oceanology (BG)
K03	Black Sea (BLKS)	2009	40	*R/V Akademik*	Institute of Oceanology (BG)
K04	Black Sea (BLKS)	2011	38	*R/V Mare Nigrum*	National Institute of Marine Geology and Geoecology (RO)
K05	Black Sea (BLKS)	2011	24	*R/V Akademik*	Institute of Oceanology (BG)
K06	Black Sea (BLKS)	2011	59	*R/V Akademik*	Institute of Oceanology (BG)
K07	Black Sea (BLKS)	2012	93	*R/V Akademik*	Institute of Oceanology (BG)
K08	Black Sea (BLKS)	2012	14	*R/V Akademik*	Institute of Oceanology (BG)
K09	Black Sea (BLKS)	2016	54	*R/V Akademik*	Institute of Oceanology (BG)
K10	Black Sea (BLKS)	2016	83	*R/V Akademik*	Institute of Oceanology (BG)
K11	Black Sea (BLKS)	2019	80	*R/V Akademik*	Institute of Oceanology (BG)
K12	Black Sea (BLKS)	2019	44	*R/V Akademik*	Institute of Oceanology (BG)
L01	Ligurian Sea (LIGS)	2008	41	*R/V Alliance*	Undersea Research Center (NATO)
L02	Ligurian Sea (LIGS)	2009	63	*R/V Alliance*	Undersea Research Center (NATO)
L04	Ligurian Sea (LIGS)	2013	25	*R/V Alliance*	Undersea Research Center (NATO)
N01	English Channel & North Sea (NORS)	2004	55	*R/V Côtes de la Manche*	Université du Littoral Côte d'Opale (FR)
N02	North Sea (NORS)	2015	52	*R/V Belgica*	Royal Belgian Institute of Natural Sciences (BL)
O01	Western Med. Sea (WMED)	2012	73	*R/V Urania*	Italian National Research Council (IT)
O02	Western Med. Sea (WMED)	2014	64	*R/V Urania*	Italian National Research Council (IT)
O03	Western Med. Sea (WMED)	2021	53	*R/V Garcia del Cid*	Institute of Marine Science (SP)

https://doi.org/10.5194/essd-2024-240
Preprint. Discussion started: 26 June 2024

Open Access Earth System Science Data Discussions

P01	Greenland Sea (GRLS)	2018	15	*R/V Alliance*	Undersea Research Center (NATO)
P03	Greenland Sea[1] (GRLS)	2021	40	*R/V Alliance*	Italian Hydrographic Institute (IT)

[1] It includes stations from the Norwegian Sea.

3. Measurements

CoASTS and BiOMaP core data comprise *in situ* and laboratory measurements performed on samples prepared in the field. The firsts include:

a. Vertical profiles of multispectral upwelling nadir radiance $L_u(z,\lambda)$, downward irradiance $E_d(z,\lambda)$, and upward irradiance $E_u(z,\lambda)$, were z indicates depth and λ the center-wavelength of each spectral band;
b. Above-water multispectral downward irradiance $E_s(\lambda)$ (often indicated as $E_d(0^+, \lambda)$ where 0^+ indicates in-air measurements) and diffuse sky irradiance $E_i(\lambda)$ recorded with a rotating shadow band operated in conjunction with an irradiance sensor;
c. Multispectral profiles of water beam attenuation $c(z,\lambda)$, absorption $a(z,\lambda)$ and backscattering $b_b((z,\lambda)$ coefficients commonly restricted to the first 25 m depth for BiOMaP and 15 m for CoASTS;
d. Profiles of water temperature $T_w(z)$ and salinity $S_w(z)$, also restricted to the first 25 m depth for BiOMaP and 15 m for CoASTS;
e. Meteorological data including wind speed W_s in addition to cloud cover C_c and sea state S_s observations.

The laboratory measurements performed on field samples, which provide data complementary to *in situ* data, are:

f. Spectral *in vivo* particulate absorption coefficients $a_{ph}(\lambda)$ for the pigmented and $a_{dt}(\lambda)$ for the non-pigmented particles;
g. Spectral CDOM absorption coefficient $a_{ys}(\lambda)$;
h. Phytoplankton pigments concentration;
i. Total suspended matter concentration *TSM*.

4. Measurement and data reduction methods

Information on measurement methods and data reduction are summarized in the following subsections.

4.1 Radiometric products

CoASTS in-water radiometric measurements of $L_u(z,\lambda)$, $E_d(z,\lambda)$, $E_u(z,\lambda)$ were performed with the Wire-Stabilized Profiling Environmental Radiometer (WiSPER) using Satlantic (Halifax, Canada) OCR/OCI-200 multispectral radiometer series. Concurrently, in air $E_s(\lambda)$ and $E_i(\lambda)$ measurements were also made with OCI-200 radiometers. In the case of BiOMaP, the equivalent measurements were performed using miniPRO and microPRO Satlantic custom designed free-fall profilers equipped with OCR/OCI-200 or alternatively OCR-507 multispectral radiometers. All radiometric quantities were measured with 6 Hz acquisition rate in spectral bands relevant for ocean color applications exhibiting 10 nm bandwidth and nominal center-wavelengths at 412, 443, 490, 510, 555, 665 and 683 nm. WiSPER data were gathered with a deployment speed of 0.1 m s^{-1}. Conversely, the deployment speed of the free-fall systems generally varied in the range of approximately 0.3-0.4 m s^{-1}. The collection of in-water radiometric measurements with low tilt and as close as possible to the surface, was always

https://doi.org/10.5194/essd-2024-240
Preprint. Discussion started: 26 June 2024

attempted to ensure best retrieval of subsurface radiometric values through the extrapolation of profile data.

The regular absolute radiometric calibration of field optical radiometers was performed at the JRC Marine Optical Laboratory using 1000W FEL lamps traceable to the National Institute of Standards and Technology (NIST) or alternatively the National Physical Laboratory (NPL). While CoASTS radiometers were re-calibrated on a six-monthly basis, BiOMaP radiometers were calibrated before and after each oceanographic campaign. Regular inter-calibrations between the JRC Marine Optical Laboratory and the National Aeronautics and Space Administration (NASA) performed within the framework of the Ocean Color component of the Aerosol Robotic Network (AERONET-OC), ensured continuous verification of the accuracy of the calibration process (Zibordi et al. 2021).

Data pre-processing included: *i.* the application of absolute calibration coefficients and immersion factors for in-water radiometers (Zibordi et al. 2004; Zibordi 2006); *ii.* the removal of in-water and in air data exhibiting tilt higher than 5° (this was confidently established from 2009 for BiOMaP $E_s(\lambda)$ and $E_i(\lambda)$); *iii*. limited to BiOMaP, the composition of successive profile data typically collected within a 5 min interval to create multi-cast profiles to increase the number of measurements per unit depth and consequently improve the accuracy of the extrapolation values; and i*v.* the correction of in-air irradiance data for the non-cosine response of collectors (see Zibordi and Bulgarelli 2007).

In agreement with consolidated protocols (*e.g.,* see IOCCG 2019), the effects of light change were minimized through normalization of each radiometric quantity with respect to above–water downward irradiance $E_s(\lambda)$ simultaneous to the in-water data. Specifically, the normalization aimed at producing radiometric quantities as if they were taken at the same time t_0 at each depth z, where t_0 was chosen to coincide with the beginning of the acquisition sequence during each cast or multi-cast.

The sub-surface quantities $L_u(0^-,\lambda)$, $E_u(0^-,\lambda)$ and $E_d(0^-,\lambda)$ were then determined at the depth $z_0 = 0$ (identified by 0^-) as the exponentials of the intercepts resulting from the least-squares linear regressions of $\ln\Im(z,\lambda)$ versus z within the extrapolation interval $z_0 < z < z_1$, where $\Im(z,\lambda)$ indicates either $L_u(z,\lambda)$, $E_d(z,\lambda)$ or $E_u(z,\lambda)$ normalized with respect to $E_s(\lambda)$ at matching times. The extrapolation interval is generally comprised between the depths $z_0 = 0.3$ and $z_1 = 5$ m and was chosen on a profile-by-profile basis with the aid of absorption and scattering profile data to identify depths best satisfying the requirement of linear decay with depth of the log-transformed radiometric data.

Outliers in the $z_0 - z_1$ depth interval generally due to wave focusing, were excluded from the extrapolation process by removing points exhibiting distance higher than $3\cdot\sigma$ from the linear regression line, where σ is the standard deviation of the differences between data points and regression line.

The $L_u(0^-,\lambda)$ and $E_u(0^-,\lambda)$ data products were corrected for self-shading and potential bottom perturbations (Zibordi et al. 2002). Additionally, limited to CoASTS data collected in the vicinity of the AAOT, corrections were applied for perturbations due to the deployment structure (Doyle and Zibordi 2002, Doyle et al. 2003). BiOMaP data, generally collected at distances from the ship of approximately 15–30 m, did not require corrections for the deployment perturbations by the structure.

In addition to $L_u(0^-,\lambda)$, $E_u(0^-,\lambda)$ and $E_d(0^-,\lambda)$ further retrieved data products are the slopes of the regression fits $K_\Im(\lambda)$ (*i.e.,* $K_l(\lambda)$, $K_u(\lambda)$ and $K_d(\lambda)$) in the extrapolation interval —

https://doi.org/10.5194/essd-2024-240
Preprint. Discussion started: 26 June 2024

so called diffuse attenuation coefficients. Derived radiometric data products are then the remote sensing reflectance $R_{rs}(\lambda)$

$$R_{\mathrm{rs}}(\lambda) = L_{\mathrm{w}}(\lambda)/E_{\mathrm{s}}(\lambda) \quad (1)$$

and the normalized water–leaving radiance $L_{\mathrm{wn}}(\lambda)$

$$L_{\mathrm{wn}}(\lambda) = R_{\mathrm{rs}}(\lambda)E_0(\lambda), \quad (2)$$

where here $E_{\mathrm{s}}(\lambda)$ refers to the value measured at time t_0, $E_0(\lambda)$ is the extra-atmospheric solar irradiance (Thuillier et al. 2003) at the mean sun-earth distance, and $L_{\mathrm{w}}(\lambda)$ is the water–leaving radiance, *i.e.,* the radiance leaving the sea and quantified just above the surface through the extrapolation process, and given by

$$L_{\mathrm{w}}(\lambda) = 0.544\, L_{\mathrm{u}}(0^-, \lambda). \quad (3)$$

where the factor 0.544 accounts for the radiance reduction across the water surface due to the change in the refractive index at the air–water interface, as determined assuming that the refractive index of seawater is independent of wavelength (Austin 1974).

Finally, supplementary derived quantity is the Q-factor at nadir $Q_{\mathrm{n}}(0^-,\lambda)$ determined by the ratio of $E_{\mathrm{u}}(0^-, \lambda)$ to $L_{\mathrm{u}}(0^-, \lambda)$ spectrally fitted to a quadratic function in the 412-555 nm spectral interval to minimize the impact of calibration and extrapolation uncertainties.

The quantities $R_{\mathrm{rs}}(\lambda)$ and $L_{\mathrm{wn}}(\lambda)$, due to the normalization with respect to $E_s(\lambda)$, benefit of a first correction for changes in illumination conditions with sun zenith, sun-earth distance and atmospheric transmittance (Mueller and Austin 1995). The additional correction performed through the application of $C_{f/Q}(\theta_0, \lambda, \tau_a, IOP)$ factors to $L_{\mathrm{wn}}(\lambda)$ and analogously to $R_{\mathrm{rs}}(\lambda)$, which leads to the determination of the final $L_{\mathrm{WN}}(\lambda)$ and $R_{\mathrm{RS}}(\lambda)$ data products, accounts for in-water bi-directional effects. The $C_{f/Q}$ factors are a function of the water inherent optical properties *IOP* (absorption and back-scattering coefficients), the atmospheric optical properties conveniently expressed through the aerosol optical thickness τ_{a} and the sun zenith angle θ_0. These factors were determined applying the tabulated values proposed by Morel et al. (2002) for Case 1 waters with *IOPs* solely expressed as a function of chlorophyll-*a* concentration *Chla*. It is acknowledged that this correction may be affected by large uncertainties when applied to optically complex waters.

An estimate of the uncertainties for CoASTS and BiOMaP L_{WN} and similarly R_{RS} data, was attempted and discussed in various publications (Zibordi and Voss 2010, Zibordi et al. 2011) accounting for the major uncertainties characterizing: *i.* absolute calibration coefficients and immersion factors; *ii.* correction factors for shading perturbations; *iii.* correction factors for in-water bidirectional effects; *iv.* the determination of $E_{\mathrm{d}}(0^+,\lambda)$; *v.* the quantification of $E_0(\lambda)$ when ignoring actual bandwidths; *vi.* the extrapolation process for the computation of sub-surface data; and *vii.* finally, environmental stability as a result of wave perturbations and changes in illumination conditions and seawater optical properties during profiling. In the specific case of moderately optically complex waters such as those characterizing CoASTS measurements, uncertainties affecting L_{WN} and R_{RS} are expected to approach 5% in the blue green spectral region and 7% in the red. In agreement with analyses performed for alternative radiometry methods (Gergely and Zibordi 2014), the above relative uncertainties may become significantly

https://doi.org/10.5194/essd-2024-240
Preprint. Discussion started: 26 June 2024

larger in the blue spectral region for data products from marine regions characterized by high water absorption such as the Baltic Sea.

Quality indices for radiometric products were determined during data processing in view of supporting an evaluation of their accuracy. These include: *i*. the ratio $Q_n(0^-,412)/Q_n(1,412)$ of Q_n values determined at 0^- and 1 m depth at the 412 nm center-wavelength (hereafter indicated as $Q_R(412)$), whose significant deviation from 1 suggests issues in the extrapolation of sub-surface values; *ii.* the coefficient of variation of in-air downward irradiance $CV\_E_d(412)$ associated to each profile at the 412 nm center-wavelength, whose high value indicates significant cumulative perturbations by ship movement or changes in illumination conditions during profiling; *iii.* the diffuse to direct ratio of above-water downward irradiance $R_d(412)$, also determined at the 412 nm center-wavelength whose high values indicate poor illumination conditions likely due to high sun zeniths or cloudiness.

4.2 Absorption and attenuation from profile data

Measurements of beam attenuation $c_{t\text{-}w}(z,\lambda)$ and absorption $a_{t\text{-}w}(z,\lambda)$ coefficients of seawater, excluding the contribution of pure seawater, were determined from measurements performed using AC9s instruments from WET Labs Inc. (Philomath, Oregon) with 25 cm path-length and nine spectral bands 10 mn wide at the 412, 440, 488, 510, 555, 630, 650, 676 and 715 nm center-wavelengths. The values of $c_{t\text{-}w}(z,\lambda)$ and $a_{t\text{-}w}(z,\lambda)$, in agreement with the scheme proposed by the instrument manufacturer (WET Labs 1996.), were corrected for the effects of differences in temperature T_w and salinity S_w characterizing field measurements with respect to laboratory calibrations. These corrections were performed using $T_w(z)$ and $S_w(z)$ profile data simultaneously performed with the AC9 ones.

AC9 absorption coefficients need correction for the finite acceptance angle of the detector and the non-completely reflective surfaces of the absorption measurement chamber, both preventing the collection of the whole scattered light and naturally leading to an overestimate of $a_{t\text{-}w}(z,\lambda)$. These corrections were performed by removing a variable percentage of the scattering coefficient $b_{t\text{-}w}(z,\lambda)$ estimated from $c_{t\text{-}w}(z,\lambda)$ and $a_{t\text{-}w}(z,\lambda)$ at each λ, assuming the absorption coefficient of particulate and dissolved material is zero at the reference wavelength λ_0=715 nm and the shape of the volume scattering function is spectrally independent (Zaneveld et al. 1992).

In addition to regular instrument calibration and maintenance by the manufacturer, systematic AC9s pure water calibrations offsets were determined during each CoASTS campaign and, at the beginning and completion of each BiOMaP campaign. The absorption and scattering offsets between the reference manufacturer's calibrations and those performed in the field were applied as corrections factors. In the presence of appreciable offsets between successive field calibrations performed during the same campaign, differences were linearly interpolated over time.

Automated quality control was applied to each data record to verify the spectral and spatial (*i.e.,* vertical) consistency aiming at identifying those measurements affected by perturbations caused by bubbles or large particles flowing into the AC9 measurement chambers. Specifically, $c_{t\text{-}w}(z,\lambda)$ and $a_{t\text{-}w}(z,\lambda)$ spectra exhibiting pronounced differences with respect to those characterizing the mean of profile spectra determined through a spectral consistency test, or pronounced changes with respect to depth at any λ identified through a spatial consistency test, were removed. The statistical parameters characterizing such a filtering process were tuned for profile data typical of individual campaigns in view of minimizing the potential for removing good measurements.

https://doi.org/10.5194/essd-2024-240
Preprint. Discussion started: 26 June 2024

The quality controlled $c_{t\text{-}w}(z,\lambda)$ and $a_{t\text{-}w}(z,\lambda)$ data were successively binned at 1 m resolution and retained when the depth d_b assigned to the center of the bin determined from the mean of the actual depths of individual measurements satisfies the condition $d_b = d_n \pm 0.25 \cdot d_i$, where d_n is the nominal depth of the center of the bin and d_i the bin width.

An uncertainty of 0.005 m^{-1} is tentatively assumed to affect AC9 measurements (Twardowski *et al.* 2001).

4.3 Backscattering from profile data

In situ vertical profiles of backscattering coefficients $b_b(z,\lambda)$ were determined using measurements performed with HydroScat-6 instruments from HOBI Labs Inc. (Tanque Verde, Arizona) in six bands 10 nm wide at the 442, 488, 510, 555, 620 and 676 (or 671) nm center-wavelengths. Specifically, the values of $b_b(z,\lambda)$ were derived applying the conversion factor χ=1.08 to measurements of the volume scattering function $\beta(z,\psi,\lambda)$ performed at the sole scattering angle ψ=140° (Maffione and Dana 1997). The derived backscattering values were successively corrected for the water scattering and absorption applying the factor

$$\sigma_C(z,\lambda) = \exp\left[k_e(\lambda)\left(a(z,\lambda) + 0.4b(z,\lambda)\right)\right] \quad (4)$$

where $a(z,\lambda)$ and $b(z,\lambda)$ (with $b(z,\lambda)=c(z,\lambda)-a(z,\lambda)$) were obtained from AC9 measurements adding the pure water absorption and scattering coefficients, respectively, while the instrument specific spectral factors $k_e(\lambda)$ were those determined by the manufacturer during the initial calibration. Salinity corrections were applied considering 'Fresh water' b_{bw} from Morel (1974) for the Black Sea and Baltic Sea measurements, and the 'Salt water' b_{bw} from Morel (1974) for the other measurements. This solution, with respect to the use of actual salinity values, may lead to misestimates of b_{bw} generally not exceeding 2% at 443 nm for the Baltic Sea and Black Sea.

Equivalent to AC9 measurements, automated quality control was also applied to $b_b(z,\lambda)$ data to remove measurements exhibiting poor spectral and spatial (*i.e.,* vertical) consistency. By tuning the parameters defining the filtering process, spectra of $b_b(z,\lambda)$ exhibiting extreme differences with respect to the mean of profile spectra, or very high changes with depth at any λ, were removed. Quality controlled $b_b(z,\lambda)$ data were also binned at 1 m resolution adopting the same criteria applied for $a(z,\lambda)$ and $c(z,\lambda)$. .

Annual calibrations performed at HOBILabs were complemented by pre-field calibrations performed at the JRC Marine Optical Laboratory.

Whitmire et al. (2007) estimated uncertainties of 0.0007 m^{-1} for measurements of $b_{bp}(z,\lambda)$ (*i.e.,* $b_b(z,\lambda)$ minus the backscattering of pure water) performed with HydroScat-6 instruments.

4.4 Absorption of particulate matter determined from discrete water samples

In vivo absorption coefficients $a_p(z,\lambda)$ of aquatic particles from water samples at discrete depths z were determined using the Transmission and Reflection (*T-R*) method proposed by Tassan and Ferrari (1995). This method was shown appropriate for any particle type, including highly back-scattering mineral particles or highly absorbing sediments. The method was implemented on a Perkin Elmer Lambda-19 and from 2004 on a Lambda-900, dual beam spectrometers equipped with integrating spheres.

Samples of water particles were collected filtering water volumes on Wattman GF/F glass fibre filters with nominal pore size of 0.7 µm. Samples from the field were preserved in liquid

https://doi.org/10.5194/essd-2024-240
Preprint. Discussion started: 26 June 2024

nitrogen until laboratory analysis. The absorption coefficient $a_p(z,\lambda)$ of the equivalent particle suspension in the 400-750 nm spectral range with 1 nm resolution was determined from

$$a_p(z,\lambda) = 2.3\, A_s(z,\lambda)\, (F_a / V_w(z))^{-1} \quad (5)$$

where $V_w(z)$ is the volume of filtered water, F_a the filter clearance area and $A_s(z,\lambda)$ the equivalent particle suspension absorbance obtained with the *T-R* method.

The pigmented $a_{ph}(z,\lambda)$ and non-pigmented $a_{dp}(z,\lambda)$ fractions of the particulate absorption coefficient $a_p(z,\lambda)$ were obtained bleaching the sample using a solution of sodium hypochlorite (NaClO). The solution rapidly acts on pigment molecules and slowly on detritus making possible a selective analysis of the two absorption components. A description of the NaClO bleaching technique is presented in Tassan and Ferrari (1995) and in Ferrari and Tassan (1999).

Focused studies on the accuracy of the *T-R* method are given in Tassan and Ferrari (1995) and in Tassan et al. (2000). Still, comprehensive uncertainty estimates for $a_{ph}(z,\lambda)$ and $a_{dp}(z,\lambda)$ are not available. Nevertheless, dedicated analysis addressed the reproducibility of in vivo particulate absorption measurements performed with the *T-R* method (see Zibordi et al. 2002). These investigated: *i*. the duplicate analysis of the same sample (*i.e.*, each sample was analysed twice) and *ii*. the analysis of duplicate samples (*i.e.*, duplicate samples obtained from the same water volume). Results for duplicate analysis of the same samples showed mean absolute percent differences of 2.9±2.3% at 443 nm with $a_p(z,443)$ = 0.082±0.042 m^{-1} and increasing up to 7.4±6.0% at 555 nm with $a_p(z,555)$ = 0.023±0.011 m^{-1}. These differences are attributed to: *i.* method sensitivity, and *ii*. slight variations in the mechanical re-positioning of the sample in front of the aperture of the integrating sphere combined with spatial non-homogeneities of particles distribution on the filter.

The analysis of duplicate samples showed mean absolute percentage differences of 8.9±5.9% at 443 nm with $a_p(z,443)$ = 0.090±0.049 m^{-1} and of 9.8±7.0% at 555 nm with $a_p(z,555)$ = 0.024±0.012 m^{-1}. The former differences, increased by a few percent with respect to those given for the duplicate analysis of samples, are justified by: *i.* unavoidable differences in replicates due to inhomogeneity affecting the particles distributions on filters; and also *ii*. unavoidable differences in the water volumes used to produce the samples. It is mentioned that an intrinsic error in the estimate of the actual particle absorption coefficients results from the application of GF/F filters with nominal pore size of 0.7 µm. In fact these filters do not allow bacteria and the fraction of mineral particles with diameter lower than 0.7 um to be accounted for. However, the absorption of these small mineral particles is generally negligible compared to the total absorption, while the absorption of bacteria is almost 10 times lower than that of algal cells.

4.5 Absorption of CDOM determined from discrete water samples

The absorption coefficient $a_{ys}(z,\lambda)$ of CDOM at depth z was determined applying the method detailed in Ferrari et al. (1996) using a Perkin Elmer Lambda-12 dual-beam spectrometer. Samples were prepared by filtering water volumes on Millipore 0.22 µm pore size cellulose filters and adding a solution of 10 gl^{-1} of NaN_3 to the filtered water to prevent bacteria growth (typically 1 ml of the solution was added to 100 ml of filtered water). CDOM samples were preserved at approximately 4^0C in an amber glass bottle until laboratory analysis. The spectrometric measurements, generally carried out within a few days from the completion of the measurement campaign, were performed with 1 nm resolution in the 350-750 nm spectral region.

https://doi.org/10.5194/essd-2024-240
Preprint. Discussion started: 26 June 2024

Measurements were performed placing a 10 cm quartz cuvette containing pure milli-Q water in the optical path of the reference beam, and a 10 cm quartz cuvette containing the CDOM sample in the optical path of the sample beam.

The spectral absorption coefficient $a_{ys}(z,\lambda)$ was computed from the measured absorbance $A_{ys}(z,\lambda)$ resulting from the difference between the sample absorbance and the reference absorbance (Ferrari et al., 1996), as

$$a_{ys}(z,\lambda) = 2.3\, A_{ys}(z,\lambda)\, L_c^{-1} \quad (6)$$

where L_c is the pathlength of the cuvette (10 cm for both CoASTS and BiOMaP sample analysis).

The absorption coefficients are corrected for the background by subtracting to $a_{ys}(z,\lambda)$ the mean of the $a_{ys}(z,\lambda_i)$ for $\lambda_i \in$ 670-680 nm, assuming CDOM does not absorb in the red.

For $a_{ys}(z,\lambda)$, also, comprehensive uncertainty values are not available. Still, the reproducibility of $a_{ys}(z,\lambda)$ (see Zibordi et al. 2002) was also investigated through: *i.* duplicate analysis of the same samples; and *ii.* analysis of duplicate samples. The duplicate analysis of the same samples showed average absolute percent differences varying as a function of the absorption value from 10.1±7.3% at 412 nm with $a_{ys}(z,412)$=0.168±0.037 m^{-1} up to 24.2±19.8% at 555 nm with $a_{ys}(z,555)$=0.015±0.005 m^{-1}. These differences are mostly ascribed to the precision of the method. The analysis of the duplicate samples showed expected augmented average absolute percent differences when compared to duplicate analysis of samples, varying from 12.1±6.3% at 412 nm with $a_{ys}(z,412)$=0.175±0.038 m^{-1} up to 30.3±23.8% at 555 nm with $a_{ys}(z,555)$=0.018±0.005 m^{-1}. The latter increased values are largely justified by differences between samples.

It is finally mentioned that the use of 0.22 µm pore size filters to produce CDOM samples, when the 0.7 µm pore size filters are applied for the quantification of particle absorption coefficients, suggests that the overall absorption budget cannot be fully resolved. In fact, as already anticipated, bacteria and very small mineral particles having size between 0.2 and 0.7 µm are not counted in the absorption analysis.

4.6 Pigments concentration

Phytoplankton pigment concentrations were determined by using High Performance Liquid Chromatography (HPLC) with the method proposed by Van Heukelem and Thomas (2005). Exceptions are the samples collected before 2000 for which the method proposed by Jeffrey et al. (1997) was applied.

The analysis were performed on samples of particulate matter retained on GF/F filters with a nominal pore size of 0.7µm: this choice is justified by the diameter of living phytoplankton cells generally higher than 1 µm (Stramsky and Kiefer, 1991). After filtration, samples were preserved in liquid nitrogen until laboratory analysis.

Following Van Heukelem and Thomas (2005), the samples were transferred to vials with 3 mL 95% acetone and vitamin E as internal standard. Samples were then disrupted using a vortex mixer, sonicated on ice, extracted at 4°C for 20 h, and mixed again. The samples were successively filtered through 0.2 µm Teflon syringe filter into HPLC vials and placed in the cooling rack of the HPLC system. Buffer and sample were injected in the HPLC (Shimadzu LC-10A or alternatively an HP-1100, systems) in the 5/2 ratio using a pre-treatment program and mixing in the loop before injection.

https://doi.org/10.5194/essd-2024-240
Preprint. Discussion started: 26 June 2024

The list of pigments systematically analysed at the JRC Marine Optical Laboratory or alternatively at DHI A/S (Hørsholm, Denmark) includes: chlorophyll a (resulting from the sum of divinyl- and monovinyl-chlorophyll a), chlorophyll b, chlorophyll c_1+c_2, chlorophyllide a, fucoxanthin, diadinoxanthin, β-carotene, zeaxanthin, alloxanthin, 19'-butanoyloxyfucoxanthin, 19'-hexanoyloxyfucoxanthin and diatoxanthin.

Various inter-comparisons of HPLC methods performed within the framework SeaWiFS HPLC Analysis Round-Robin Experiments (SeaHARRE) organized by NASA with the JRC participation, demonstrated the capability of various laboratories to achieve differences lower than 6% in the determination of total chlorophyll a concentration (*i.e.*, the sum of chlorophyll a and chlorophyllide a) and lower than 25% for the other ancillary pigments characterizing marine waters (Hooker et al. 2010).

4.7 Total suspended matter concentration

The concentration of total suspended matter, *TSM,* was obtained from the net weight of the particulate material collected on filters following the method detailed in Van der Linde (1998) as an evolution of that proposed by Strickland and Parsons (1972). Samples were produced by filtering volumes of water on GF/F 0.7 µm nominal pore size filters previously baked at 450^0C for 1 hour, pre-washed, dried for 1 hour at 75^0C and finally pre-weighted on a electrobalance. The filters (*i.e.*, filtration area and border) with water particles were washed with distilled water and stored at -18^0C for successive laboratory analysis. Before final weighting, the filters were dried at 75^0C for 1 hour, and then temporarily stored in a desiccator.

The concentration of total suspended matter was calculated from

$$TSM(z) = [(W_f(z) - W_s(z)) - w_b]V(z)^{-1} \quad (7)$$

where $W_f(z)$ is the weight of the filter before filtration, $W_s(z)$ is the weight of the sample filter after filtration, $V(z)$ is the volume of the filtered water and w_b is a correction term introduced to account for variations in the weight of the filter sample due to changes in environmental conditions between the two weightings steps. The values of w_b were determined from 'blank' filters (*i.e.,* GF/F filters completely conditioned, not used for water filtration, but exposed to the same processes of the sample filters: transportation to the measurement site and back, storage in the freezer, drying). The w_b values applied in Eq. 7, are the differences between the average final weight of 'blank' filters and their original average weight.

The use of GF/F filters with 0.7 µm nominal pore size for *TSM* analysis can lead to an underestimate of total suspended matter due to the loss of particles with diameter lower that 0.7 µm. However, it is recognized that the filter rinsing for salt removal and the filter conditioning after filtration before final weighting, can induce errors certainly much larger than the mass of particles with diameter lower than 0.7 µm.

An analysis of measurement reproducibility performed with duplicate samples showed mean percent difference equal to 13.9±13.4% with $TSM(z)$=0.86±0.40 mg·l^{-1}. The largest differences between duplicate samples (*i.e.,* larger than 30%) were observed with values of $TSM(z)$ lower than approximately 0.5 mg·l^{-1}. This is explained by the intrinsic uncertainty affecting sample preparation (*i.e.,* water sample non-homogeneity and filter rinsing).

https://doi.org/10.5194/essd-2024-240
Preprint. Discussion started: 26 June 2024

4.8 Salinity and temperature

Profiles of salinity $S_w(z)$ and temperature $T_w(z)$ measurement were performed with SBE 19-plus Conductibility-Temperature-Depth (CTD) sensors from Sea-Bird Scientific (Bellevue, Washington). These devices were calibrated by the manufacturer approximately on a two-year basis. Uncertainties are tentatively expected to be within 0.01 ‰ for salinity and 0.01ºC for temperature.

Equivalent to $a(z,\lambda)$, $c(z,\lambda)$ and $b_b(z,\lambda)$ profiles, automated quality control was also applied to $S_w(z)$ and $T_w(z)$ data to remove measurement artefacts. By trimming filtering parameters to individual campaigns, values of $S_w(z)$ and $T_w(z)$ exhibiting extreme changes with respect to depth, were removed. Quality checked $S_w(z)$ and $T_w(z)$ data were binned at 1 m resolution adopting the same criteria already applied for $a(z,\lambda)$, $c(z,\lambda)$ and $b_b(z,\lambda)$.

4.9 Meteorological and environmental observations

Among the meteorological quantities and observations recorded during each measurements station the wind speed W_s, sea state *Ss* and cloud cover *Cc* are included in the data set.

5. The near-surface CoASTS and BiOMaP dataset (CoASTS-BiOMaP)

CoASTS-BiOMaP data are accessible at https://doi.org/10.1594/PANGAEA.968716 in tabular form and include the near-surface data products from CoASTS and BiOMaP measurements of relevance for the validation of satellite ocean color data and the development of bio-optical algorithms (because of this, the depth dependence is omitted for convenience in the discussion of results in the following sections). All spectral data products are restricted to the nominal center-wavelengths 412, 443, 490, 510, 555, 665 nm, unless diversely specified. CoASTS data products are only provided from December 1998 when full standardization of measurement and processing was put in place. In addition, station data were excluded from CoASTS-BiOMaP when the $L_{WN}(\lambda)$ or $K_d(\lambda)$ radiometric products did not satisfy basic quality control criteria (*e.g.*, $L_{WN}(\lambda)$ exhibited spectra with unexplained shape or amplitude, or $K_d(\lambda)$ showed values lower that those expected for pure marine water). Furthermore, poor quality of any data product other than radiometric, also implied its exclusion from CoASTS-BiOMaP.

Table 3 provides a comprehensive list of the quantities included in the CoASTS-BiOMaP dataset: each one is identified by a convenient symbol and a brief description and the physical units. A summary of the average values of the major bio-optical and hydrographic quantities determined for the various marine regions is provided in Table 4. These are: the diffuse attenuation coefficient K_d, the water absorption coefficient (from discrete sample analysis, pure water contribution excluded) a, the backscattering coefficient (water contribution included) b_b, at the 490 nm center-wavelength (488 nm for b_b); the concentrations of total chlorophyll-a *Chla* and total suspended matter *TSM*; and the salinity S_w. All quantities exhibit ample differences across the various marine regions. Notable, variations in $K_d(490)$ exceed one order of magnitude between the Eastern Mediterranean (EMED) and the Baltic Sea (BLTS) waters (*i.e.,* varies from 0.037 to 0.495 m^{-1}).

Figure 3 displays BioMaP and CoASTS $L_{WN}(\lambda)$ spectra for the different marine regions. Spectra clearly indicate diverse bio-optical features for the different regions. They span from the highly oligotrophic Eastern Mediterranean Sea (EMED) showing maximum values in the blue region to the optically complex Baltic Sea (BLTS) dominated by the presence of high concentrations of CDOM as expressed by low values of L_{WN} in the blue spectral region. Between these, there are marine regions exhibiting diverse bio-optical complexity due to different

https://doi.org/10.5194/essd-2024-240
Preprint. Discussion started: 26 June 2024

Open Access Earth System Science Data Discussions

concentrations of optically significant constituents. Notably, spectra from the North Sea (NORS) indicate the presence of relatively high concentration of sediments, while spectra from the Black Sea (BLK) and the northern Adriatic Sea (AAOT) suggest bio-optical conditions determined by the presence of variable concentrations of suspended and coloured dissolved organic matter determining L_{WN} maxima at the 510 or 555 nm center-wavelengths.

Table 5 provides the mean spectral values and related standard deviations of $Q_n(\lambda)$ for the various marine regions as determined from radiometric profiles performed during near clear sky conditions determined by $Cc \leq 1/4$. These naturally exhibit some spectral dependence varying with the water type. For instance, $Q_n(\lambda)$ from the Eastern Mediterranean Sea (EMED) exhibit almost spectrally constant mean values approaching 4 sr in the 412-555 nm spectral interval and of approximately 5 sr at 665 nm. Conversely, regions such as the northern Adriatic Sea (AAOT) exhibit mean values approaching 4.5 sr with some spectral dependence in the 412-555 nm spectral region, and also a mean value of 5 sr at 665 nm.

Figure 4 displays the $a_{ph}(\lambda)$ spectra for the CoASTS and BioMaP regions. Notable is the increase in the values of mean $a_{ph}(443)$ from 0.007 m^{-1} for the Eastern Mediterranean Sea (EMED) to 0.220 m^{-1} for the North Sea (NORS). The peculiar spectra shown by North Sea stations off the Belgian coast exhibiting a_{ph} values higher at 412 nm than at 443 nm (see panel for NORS data in Fig. 4), are explained by high concentrations of pheophytin leading to an increase of the absorption coefficient toward 412 nm.

Figure 5 displays the comparison of the near surface absorption coefficients (pure water excluded) determined from AC9 measurements at the center-wavelength of 440 nm, $a_{t\text{-}w}$(AC9), versus the equivalent absorption coefficients determined from water samples, $a_{t\text{-}w}$(sample)= $a_{ph}(443)+a_{dt}(443)+a_{ys}(443)$. Results suggest an increasing underestimate of $a_{t\text{-}w}$(AC9) with a decrease in absorption. This is highlighted by the scatter plots of data from the Eastern Mediterranean Sea (EMED) exhibiting an underestimate exceeding 80% with values of $a_{t\text{-}w}$(samples) generally lower than 0.1 m^{-1}. Conversely, the Baltic Sea (BLTS) shows outstanding agreement between the compared quantities with absorption values comprised in the range of 0.2-1.2 m^{-1}. These differences between $a_{t\text{-}w}$(AC9) and $a_{t\text{-}w}$(samples) absorption values could be explained by an incomplete correction of the perturbing effects due to finite acceptance angle of the detector, the non-fully reflective surface of the AC9 absorption chamber (*i.e.*, the two short 25 cm path-length tube) and also by the non-negligible absorption of particles at the reference wavelength λ_0=715 nm applied for scattering corrections.

Table 3. The CoASTS-BiOMaP data set: quantities identified by symbols, description of quantities and related units.

Symbol	***Description***	***Units***	***Details***
Station_ID	Station identifier	Code	*Gccssii*[(1)]
Date&Time	Date and time	GMT	*yyyy-mm-dd*T*hh:mm:ss*[(2)]
Lon	Longitude	Degrees	
Lat	Latitude	Degrees	
Sz	Sun zenith	Degrees	
Sa	Sun azimuth	Degrees	
$L_u(\lambda)$	Upwelling radiance at depth 0^-	W m^{-2} nm^{-1} sr^{-1}	at nominal λs[(3)]
$E_d(\lambda)$	Downward irradiance at depth 0^-	W m^{-2} nm^{-1}	at nominal λs[(3)]
$E_u(\lambda)$	Upward irradiance at depth 0^-	W m^{-2} nm^{-1}	at nominal λs[(3)]
$K_L(\lambda)$	Diffuse att. coeff. from $L_u(z,\lambda)$	m^{-1}	at nominal λs[(3)]

https://doi.org/10.5194/essd-2024-240
Preprint. Discussion started: 26 June 2024

$K_d(\lambda)$	Diffuse att. coeff. from $E_d(z,\lambda)$	m^{-1}	at nominal $\lambda s^{(3)}$
$K_u(\lambda)$	Diffuse att. coeff. from $E_u(z,\lambda)$	m^{-1}	at nominal $\lambda s^{(3)}$
$E_s(\lambda)$	Downward irradiance at depth 0^+	W m^{-2} nm^{-1}	at nominal $\lambda s^{(3)}$
$Q_n(\lambda)$	Q-factor an nadir at depth 0^-	sr	at nominal $\lambda s^{(3)}$
$R_{RS}(\lambda)$	Remote sensing reflectance at depth 0^+	sr^{-1}	at nominal $\lambda s^{(3)}$
$L_{WN}(\lambda)$	Normalized water-leaving rad. at depth 0^+	W m^{-2} nm^{-1} sr^{-1}	at nominal $\lambda s^{(3)}$
$Q_R(412)$	Ratio of $Q_n(412)$ at depth 0- to $Q_n(1, 412)$ at depth 1 m	–	
$R_d(412)$	Ratio of the diffuse $E_i(412)$ to direct $[E_s(412\lambda)$-$E_i(412)]$ above-water downward irradiance at 412 nm	–	
$CV\_E_d(412)$	Coefficient of variation $E_s(412)$	‰	
$E_d(412)/[1.04*E_s(412)]$	Ratio of the in-water downward irradiance Ed(412) to the above-water downward irradiance Es(412) multiplied by 1.04	–	
$K_d(490)$- $K_w(490)$	Diffuse attenuation coefficient Kd(490) minus the diffuse attenuation coefficient of pure sea water Kw(490)	m^{-1}	
$a_{ph}(\lambda)$	Abs. coeff. by pigmented particles at –0.5 m	m^{-1}	at nominal $\lambda s^{(3)}$
$a_{dt}(\lambda)$	Abs. coeff. by non-pigmented part. at –0.5 m	m^{-1}	at nominal $\lambda s^{(3)}$
$a_{ys}(\lambda)$	Abs. coeff. by CDOM at –0.5 m	m^{-1}	at nominal $\lambda s^{(3)}$
$a_{t\text{-}w}(\lambda)$	Abs. coeff. from AC9 at –0.5 m	m^{-1}	at AC9 $\lambda s^{(4)}$
$c_{t\text{-}w}(\lambda)$	Beam att. coeff. from AC9 at –0.5 m	m^{-1}	at AC9 $\lambda s^{(4)}$
$b_b(\lambda)$	Backscatt. coeff. from HydroScat-6 at –0.5 m	m^{-1}	at HydroScat-6 $\lambda s^{(5)}$
$b_b(488)$ - $b_{bw}(488)$	Backscattering coefficient $b_b(488)$ minus the backscattering coefficient of pure sea water $b_{bw}(488)$	m^{-1}	
Chla	Total chlorophyll-*a* concentr. at –0.5 m [6]	µg l^{-1}	
TSM	Total suspended matter concentr. at –0.5 m	mg l^{-1}	
T_w	Temperature of seawater at –0.5 m	°C	
S_w	Salinity of seawater at –0.5 m	‰	
Ws	Wind speed	m s^{-1}	
Ss	Sea state	0-9	WMO scale
Cc	Cloud cover	0-4	Octa/2

[1] *G* indicates the site or geographic region (*V* and *W* for AAOT, *A* for Adriatic Sea, *B* for Baltic Sea, *E* for Eastern Mediterranean Sea, *K* for Black Sea, *L* for Ligurian Sea, *N* for North Sea, *O* for Western Mediterranean Sea, *I* for Iberian Shelf, *P* for Greenland Sea), while *cc* indicates the campaign number for the specific region, *ss* the station number and *ii* the cast number.
[2] The letters *yyyy* indicate the year, *mm* the month, *dd* the day *hh,* the hours and *mm* the minutes.
[3] Nominal center-wavelengths for radiometric data products are 412, 443, 490, 510, 555 are 665 nm.
[4] Center-wavelengths for AC9 data products are 412, 440, 488, 510, 555, 630, 650, 676, and 715 nm.
[5] Center-wavelengths for HydroScat-6 data products are 442, 488, 510, 555, 620, and 676 (or 671) nm.
[6] Total chlorophyll-*a* concentration indicates the sum of chlorophyllide-*a*, monovinyl- and divinyl-chlorophyll-*a*.

https://doi.org/10.5194/essd-2024-240
Preprint. Discussion started: 26 June 2024

Table 4. Mean ± standard deviations of quantities describing the bio-optical and hydrographic characteristics of the CoASTS and BioMaP marine regions: the diffuse attenuation coefficient K_d; the seawater absorption coefficient (excluding pure water contribution) a determined from discrete sample analysis; the backscattering coefficient (including pure water contribution) b_b, all at the 490 nm center-wavelength; the concentrations of total chlorophyll-a *Chla* and total suspended matter *TSM*; and finally the salinity *Sw*.

Region	$K_d(490)[m^{-1}]$	$a(490)$ $[m^{-1}]$	$b_b(488)[m^{-1}]$	$Chla[\mu g\ l^{-1}]$	$TSM[mg\ l^{-1}]$	S_w[‰]
EMED	0.037±0.023	0.031±0.013	0.0026±0.0007	0.09±0.08	0.26±0.43	38.7±0.7
WMED	0.046±0.025	0.040±0.019	0.0032±0.0009	0.30±0.37	0.31±0.22	37.8±0.4
IBSH	0.084±0.049	0.073±0.033	0.0040±0.0023	0.81±0.83	0.53±0.39	36.0±0.2
GRLS	0.097±0.062	0.082±0.032	0.0039±0.0021	0.94±1.04	0.64±0.28	34.0±1.6
LIGS	0.110±0.079	0.079±0.045	0.0078±0.0067	0.93±0.85	0.71±0.57	37.7±1.0
ADRS	0.140±0.125	0.085±0.059	0.0090±0.0067	1.25±1.32	1.14±1.45	35.6±2.3
AAOT	0.176±0.102	0.099±0.053	0.0121±0.0073	1.28±1.13	1.25±0.76	34.9±2.3
BLKS	0.219±0.254	0.131±0.130	0.0093±0.0066	1.62±3.13	1.17±1.24	16.6±1.8
NORS	0.875±0.865	0.377±0.346	0.0197±0.0160	4.23±2.27	9.96±12.52	33.7±1.4
BLTS	0.495±0.410	0.308±0.269	0.0107±0.0084	4.99±8.04	1.53±1.71	6.2±1.4

Figure 6 shows trilinear (ternary) plots of the absorption coefficients $a_{ys}(443)$, $a_{dt}(443)$ and $a_{ph}(443)$, expressed in percent of the total absorption (*i.e.*, with respect to $a_{ys}(443)+a_{dt}(443)+a_{ph}(443)$), displayed with values increasing in the counter-clockwise direction (Harris 1999). These results exhibit very few cases characterized by dominance of absorption by particles with a_{ph} and a_{dt} values close to the upper and lower right apexes, respectively. Conversely, most of the cases indicate dominance of absorption by coloured dissolved organic matter: see the a_{ys} values near the lower left apex). This is particularly evident for the oligotrophic waters of the Eastern Mediterranean Sea (EMED), and by the patterns characterizing the oligotrophic-mesotrophic waters of the Western Mediterranean Sea (WMED), the optically complex water of the Black Sea (BLKS) and the highly absorbing waters of the Baltic Sea (BLTS).

The specific results shown for the Mediterranean Sea (*i.e.*, EMED and WMED), which may suggest inconsistency with the definition of Case-1 waters (IOCCG 2000), are supported by an independent study from Pérez et al. (2016).

https://doi.org/10.5194/essd-2024-240
Preprint. Discussion started: 26 June 2024

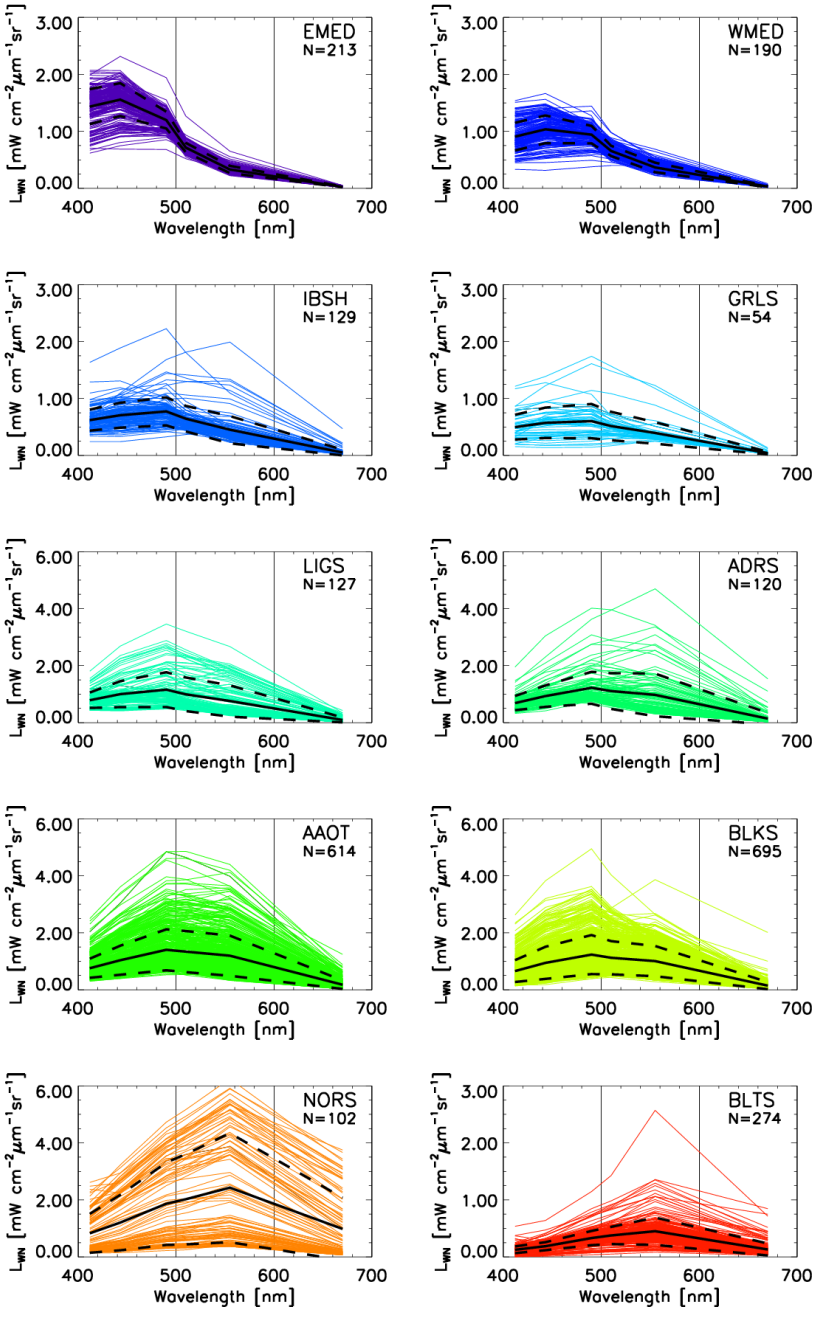

Figure 3. Spectra of $L_{WN}(\lambda)$ for the CoASTS and BioMaP geographic regions (see Table 1 for acronyms). N indicates the number of spectra. The continuous black lines indicate mean values while the dashed lines indicate ± 1 standard deviation. For convenience, the spectra are plotted in units of mW cm^{-2} μm^{-1} sr^{-1}.

https://doi.org/10.5194/essd-2024-240
Preprint. Discussion started: 26 June 2024

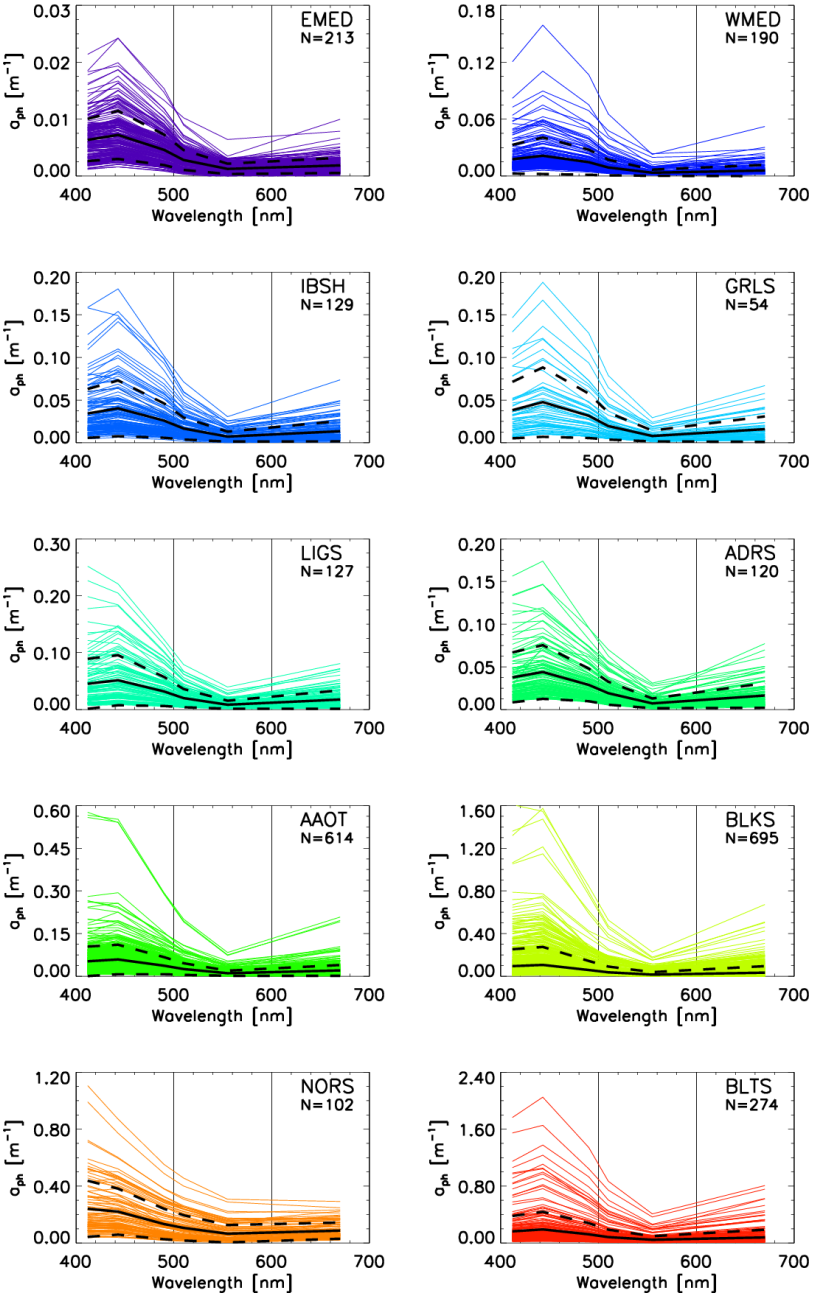

Figure 4. Spectra of $a_{ph}(\lambda)$ for the CoASTS and BioMaP marine regions. N indicates the number of spectra. The continuous black lines indicate mean values while the dashed lines indicate ± 1 standard deviation.

https://doi.org/10.5194/essd-2024-240
Preprint. Discussion started: 26 June 2024

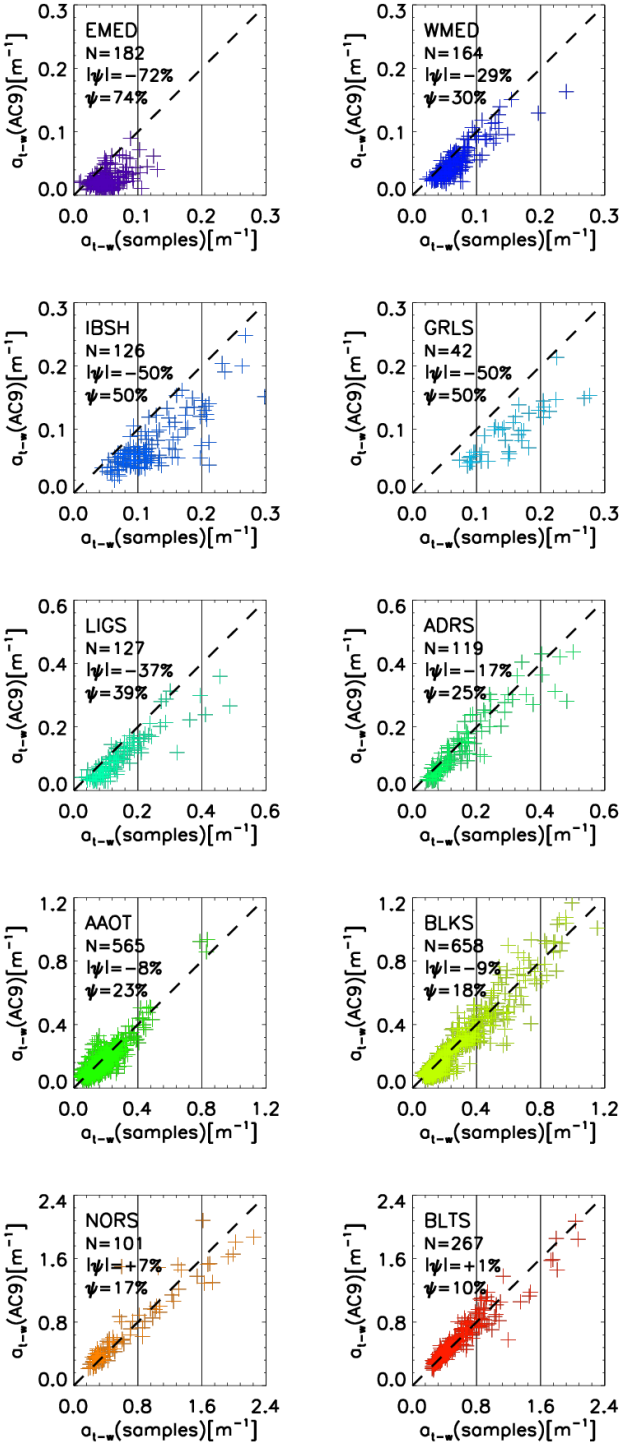

606

https://doi.org/10.5194/essd-2024-240
Preprint. Discussion started: 26 June 2024

607 Figure 5. Scatter plot of AC9 derived $a_{t\text{-}w}$(AC9) and laboratory measurements performed on
608 water samples $a_{t\text{-}w}$(samples) of the water absorption coefficient (water excluded) determined at
609 the 443 nm center-wavelength for the diverse CoASTS and BioMaP marine regions. N indicates
610 the number of samples while $|\psi|$ and ψ indicate the mean of absolute (unsigned) percent
611 differences and the mean of (signed) percent differences, respectively.

https://doi.org/10.5194/essd-2024-240
Preprint. Discussion started: 26 June 2024

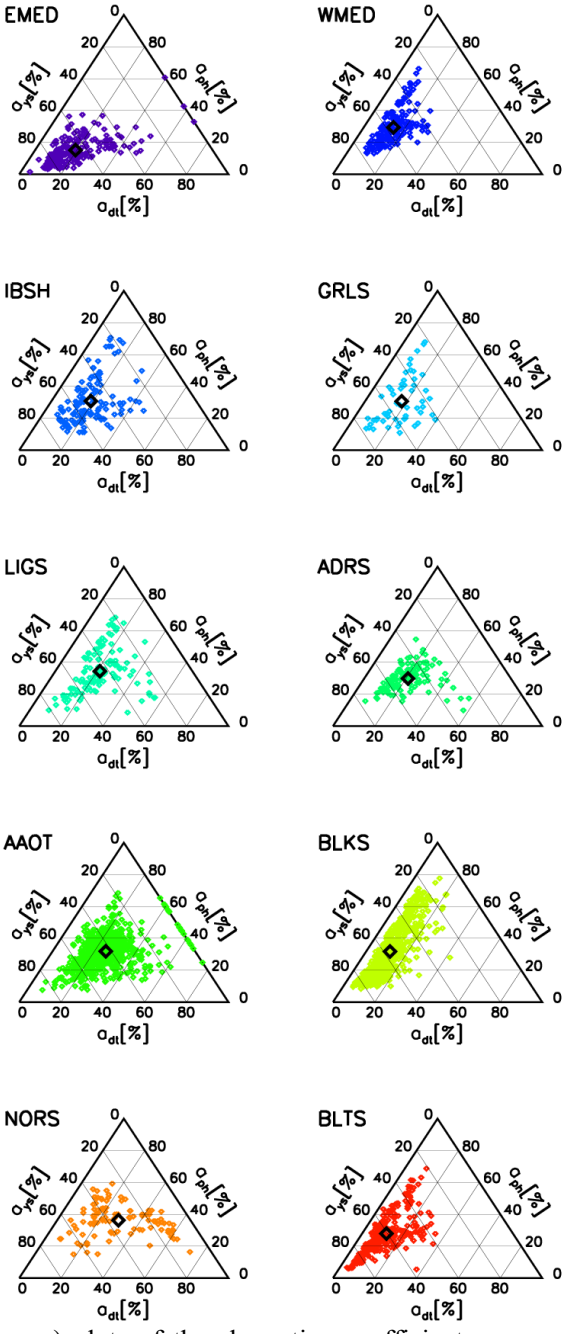

Figure 6. Trilinear (ternary) plots of the absorption coefficients a_{ys}, a_{dt} and a_{ph} expressed in percent of the total absorption (i.e., with respect to $a_{ys}+a_{dt}+a_{ph}$) at the 443 nm center-wavelength. The empty black square indicates the mean of the plotted values.

https://doi.org/10.5194/essd-2024-240
Preprint. Discussion started: 26 June 2024

Table 5. Spectral values of $Q_n(\lambda)$ in units of sr at the 412, 443, 490, 510, 555 and 670 nm center-wavelengths for the CoASTS and BioMaP marine regions, determined from in-water radiometric profiles performed with cloud cover $C_C \leq 1/4$.

Region	412	443	490	510	555	670
EMED (N=146)	3.89±0.34	3.89±0.37	3.88±0.43	3.88±0.47	3.84±0.57	4.91±1.21
WMED (N=103)	4.07±0.36	4.14±0.40	4.20±0.46	4.20±0.48	4.18±0.52	4.94±0.76
IBSH (N=87)	4.18±0.37	4.22±0.38	4.26±0.43	4.26±0.45	4.24±0.51	4.58±0.59
GRLS (N=11)	3.97±0.33	4.08±0.37	4.14±0.38	4.12±0.37	4.00±0.34	4.18±0.38
LIGS (N=53)	4.52±0.40	4.54±0.36	4.57±0.36	4.59±0.38	4.66±0.44	5.14±0.58
ADRS (N=71)	4.46±0.64	4.38±0.56	4.33±0.52	4.33±0.53	4.40±0.60	4.97±0.92
AAOT (N=372)	4.56±0.56	4.43±0.51	4.33±0.49	4.33±0.50	4.41±0.58	5.02±0.84
BLKS (N=401)	4.51±0.54	4.49±0.57	4.47±0.59	4.47±0.59	4.47±0.59	5.06±0.80
NORS (N=27)	4.71±0.61	4.72±0.59	4.71±0.56	4.68±0.55	4.61±0.52	4.92±0.51
BLTS (N=87)	4.94±0.68	5.09±0.73	5.18±0.77	5.16±0.76	4.99±0.67	5.20±0.85

Parameters determined from the exponential fit versus wavelength of $a_{dt}(\lambda)$ and $a_{ys}(\lambda)$, and the power law fit of $b_b(\lambda)$ versus wavelength, are provided in Tables 6-8. Specifically, the spectral values of $a_{dt}(\lambda)$ and $a_{ys}(\lambda)$ were fitted within the 412–665 nm spectral interval using

$$a_{dt}(\lambda) = A_{dt} \exp(-S_{dt}(\lambda - 412)) + B_{dt} \quad (8)$$

and

$$a_{ys}(\lambda) = A_{ys} \exp\left(-S_{ys}(\lambda - 412)\right) + B_{ys}, \quad (9)$$

where A_{dt} and A_{ys} indicate the absorption coefficients fitted at 412 nm, S_{dt} and S_{ys} the slope of the exponential function, and, B_{dt} and B_{ys} account for the background.

Conversely, the spectral values of $b_b(\lambda)$ at the center-wavelengths λ=442, 488, 510, 550 and 620 nm (excluding 676 µm due to potential perturbations by fluorescence), were fitted using

$$b_b(\lambda) = A_b\ (\lambda/442)^{-S_b}, \quad (10)$$

where A_b indicates the backscattering coefficient at 442 nm and S_b the slope of the power law function.

Table 6 shows mean values of the slope S_{dt} varying from 0.009 nm^{-1} for the Eastern Mediterranean Sea (EMED) up to 0.013 for the North Sea (NORS). Values of the bias B_{dt} naturally increase with A_{dt}: the largest value of B_{dt}= 0.067 m^{-1} is observed for the North Sea (NORS) that also exhibits the highest value of A_{dt}= 0.288 m^{-1} among those shown in Table 6. Residuals R_{dt}, which also increase with A_{dt}, are quite minor suggesting a general good performance of the exponential fitting function.

Table 7 shows mean values of the slope S_{ys} varying from 0.011 nm^{-1} for the Eastern Mediterranean Sea (EMED) up to 0.019 nm^{-1} for the Baltic Sea (BLTS). The systematic negative

https://doi.org/10.5194/essd-2024-240
Preprint. Discussion started: 26 June 2024

biases B_{ys} across all marine regions are likely explained by the choice of zeroing the original spectra of absorption coefficients using values averaged in the 670-680 nm spectral interval. High residuals B_{ys} = 0.029 m^{-1} are observed for the Baltic Sea. This is likely explained by a decreased performance of Eq. 9 when fitting spectra of absorption coefficients exhibiting values approaching or exceeding 1 m^{-1} at 412 nm. Still, all residuals B_{ys} expressed in percent of A_{ys} vary between 0.3 and 0.5%, except for the East Mediterranean Sea (EMED) showing a value of 0.9%.

As expected, also the values of S_b largely vary across the CoASTS and BioMaP marine regions: in particular they exhibit values of 2.66 μm^{-1} for the East Mediterranean Sea (EMED), 2.06 μm^{-1} for the Iberian Shelf (IBSH) and 0.55 μm^{-1} for the North Sea (NORS). This is likely explained by an increase of the average particles size when going from the oligotrophic East Mediterranean Sea to the eutrophic and more sediment loaded North Sea.

Figure 7 shows the distribution of *Chla* across the CoASTS and BiOMaP marine regions. Notable are the very low concentrations characterizing the oligotrophic waters of Eastern Mediterranean Sea (EMED) exhibiting mean values of 0.09 $\mu g\ l^{-1}$, while the North Sea (NORS) and Baltic Sea (BLKS) exhibit mean values in the range of 4-5 $\mu g\ l^{-1}$. Also, an apparent log-normal distribution of the *Chla* is confirmed for the CoASTS and BiOMaP data sets.

Table 9 provides the mean specific absorption coefficients $a_{ph}^{*}(443)$ determined by the ratio of $a_{ph}(443)$/*Chla* across the various CoASTS and BioMaP marine regions. These mean values of $a_{ph}^{*}(443)$ vary from 0.047 $m^2\ mg^{-1}$ in the Baltic Sea (BLT) to 0.098 in the Eastern Mediterranean Sea. It is warned that these latter values could be challenged by increased uncertainties in the determination of both $a_{ph}(443)$ and *Chla* in very oligotrophic waters.

Table 6. Parameters A_{dt}, S_{dt} and B_{dt} of the exponential fitting function (see Eq. 8) applied to the values of $a_{dt}(\lambda)$. The quantity R_{dt} indicates the spectral average of absolute differences between actual and fitted values (i.e., absolute residuals).

Region	A_{dt} [m^{-1}]	S_{dt} [nm^{-1}]	B_{dt} [m^{-1}]	R_{dt} [m^{-1}]
EMED (N=213)	0.010±0.006	0.009±0.002	0.002±0.001	0.0000
WMED (N=189)	0.009±0.004	0.012±0.001	0.003±0.001	0.0000
IBSH (N=129)	0.024±0.022	0.011±0.001	0.006±0.005	0.0001
GRLS (N=54)	0.024±0.014	0.012±0.002	0.007±0.004	0.0000
LIGS (N=126)	0.032±0.026	0.011±0.002	0.007±0.004	0.0001
ADRS (N=120)	0.042±0.057	0.012±0.001	0.009±0.011	0.0000
AAOT (N=614)	0.048±0.031	0.012±0.001	0.009±0.005	0.0000
BLKS (N=695)	0.034±0.057	0.011±0.002	0.005±0.008	0.0001
NORS (N=102)	0.288±0.377	0.013±0.001	0.067±0.094	0.0005
BLTS (N=274)	0.095±0.125	0.011±0.002	0.011±0.017	0.0003

https://doi.org/10.5194/essd-2024-240
Preprint. Discussion started: 26 June 2024

Table 7. Parameters A_{ys}, S_{ys} and B_{ys} of the exponential fitting function (see Eq. 9) applied to the values of $a_{ys}(\lambda)$. The quantity R_{ys} indicates the spectral average of absolute differences between actual and fitted values (i.e., absolute residuals).

Region	A_{ys} [m^{-1}]	S_{ys} [nm^{-1}]	B_{ys} [m^{-1}]	R_{ys} [m^{-1}]
EMED (N=205)	0.056±0.026	0.011±0.003	-0.005±0.007	0.0005
WMED (N=186)	0.059±0.019	0.013±0.003	-0.002±0.002	0.0002
IBSH (N=129)	0.093±0.036	0.014±0.003	-0.004±0.005	0.0004
GRLS (N=54)	0.107±0.027	0.014±0.003	-0.004±0.003	0.0003
LIGS (N=126)	0.091±0.052	0.014±0.004	-0.004±0.004	0.0004
ADRS (N=120)	0.114±0.058	0.016±0.002	-0.002±0.002	0.0003
AAOT (N=493)	0.132±0.059	0.017±0.004	-0.003±0.005	0.0003
BLKS (N=693)	0.205±0.122	0.017±0.002	-0.004±0.003	0.0005
NORS (N=102)	0.280±0.094	0.017±0.002	-0.004±0.002	0.0007
BLTS (N=274)	0.606±0.330	0.019±0.001	-0.004±0.003	0.0029

Table 8. Parameters A_b and S_b of the power low fitting function (see Eq. 10) applied to the values of $b_b(\lambda)$ at λ= 443, 488, 510, 555 and 620 nm for the CoASTS and BioMaP marine regions. The quantity R_b indicates the spectral average of absolute differences between actual and fitted data (*i.e.*, absolute residuals).

Region	A_b [m^{-1}]	S_b [μm^{-1}]	R_b [m^{-1}]
EMED (N=207)	0.0034±0.0008	2.95±0.69	0.0001
WMED (N=189)	0.0041±0.0009	2.55±0.42	0.0001
IBSH (N=127)	0.0051±0.0025	2.06±0.55	0.0002
GRLS (N=51)	0.0049±0.0024	2.25±0.33	0.0001
LIGS (N=126)	0.0091±0.0072	1.83±0.64	0.0002
ADRS (N=111)	0.0103±0.0071	1.74±0.57	0.0002
AAOT (N=479)	0.0136±0.0078	1.35±0.42	0.0004
BLKS (N=534)	0.0126±0.0077	1.99±0.53	0.0006
NORS (N=57)	0.0207±0.0157	0.74±0.38	0.0005
BLTS (N=256)	0.0117±0.0082	1.15±0.49	0.0003

https://doi.org/10.5194/essd-2024-240
Preprint. Discussion started: 26 June 2024

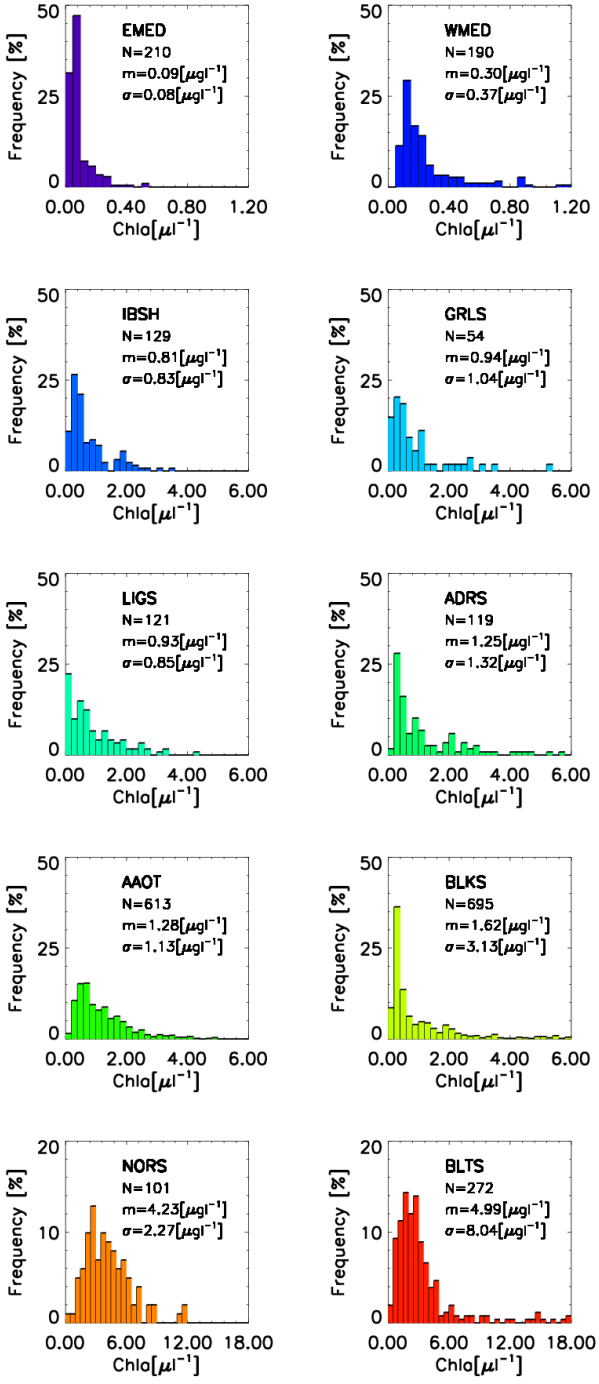

Figure 7. Occurrence of *Chla* concentrations across the CoASTS and BioMaP marine regions. N indicates the number of stations, *m* the mean values and σ the standard deviation.

https://doi.org/10.5194/essd-2024-240
Preprint. Discussion started: 26 June 2024

Table 9. Mean values of the *Chla* specific absorption coefficient a_{ph}* at 443 nm.

Region	a_{ph}* [m^2/mg^{-1}]
EMED (N=210)	0.098±0.117
WMED (N=190)	0.083±0.018
IBSH (N=129)	0.062±0.050
GRLS (N=54)	0.063±0.018
LIGS (N=121)	0.065±0.021
ADRS (N=119)	0.053±0.034
AAOT (N=613)	0.052±0.022
BLKS (N=695)	0.084±0.046
NORS (N=101)	0.061±0.108
BLTS (N=272)	0.047±0.014

6. Summary and conclusions

The CoASTS and BiOMaP measurement programs led by the JRC Marine Optical Laboratory benefitting of the collaboration of a number of European institutions and various funding programs, were conceived to support satellite ocean color applications. Between 1995 and 2022, the two programs produced time-series at the AAOT site in the northern Adriatic Sea and geographically distributed bio-optical measurements across the major European Seas. The measurements delivered by the two programs beyond December 1998 include identical quantities and are characterized by standardization of measurement methods, instruments, data processing and quality assurance/control schemes.

This work introduces the CoASTS-BiOMaP data set comprising the near surface data products from the CoASTS and BioMaP measurement programs of major relevance for satellite ocean color validation activities and bio-optical modelling.

7. Author contributions

Both authors, Giuseppe Zibordi and Jean-François Berthon, who implemented and co-led the CoASTS and BiOMaP programs, contributed to the generation of the data set and to the manuscript draft. Giuseppe Zibordi was a JRC Scientific Officer since the conception and up to the end of the CoASTS and BiOMaP programs.

8. Competing interests

Both authors declare no competing interest.

9. Data availability

Interested researchers can download the CoASTS-BiOMaP data set at https://doi.pangaea.de/10.1594/PANGAEA.968716 (Zibordi and Berthon, 2024). The original field measurements leading to the creation of this data set are currently not publicly available. However, by endorsing the EU Policy Goals and the JRC Open Data principles (A. Friis-Christensen, J. P. Triaille, *JRC Data Policy,* EUR 27163 EN, Publications Office of the European Union, Luxembourg, 2019, ISBN 978-92-76-08380-1, doi:10.2760/637912,

https://doi.org/10.5194/essd-2024-240
Preprint. Discussion started: 26 June 2024

JRC115832), these field measurements may be obtained from the authors upon a reasonable request.

10. Acknowledgments

The technical contributions to field measurements and laboratory analysis of many JRC and international colleagues are fully acknowledged: Cristina Targa, Stefania Grossi, Dirk Van der Linde, Lukasz Jankowski, Lyudmila Kamburska, Davide D'Alimonte, Marco Talone, Pietro Sciuto, Ilaria Cazzaniga, Jean Verdebout, Elisabetta Canuti, Alessandro Marchetti, Violeta Slabakova, Natalia Slabakova, Carolina Sa', Simone Colella, Gianluca Volpe, Seppo Kaitala, Jukka Seppala, Aleksandra Mazur.

11. Funding support

Direct or indirect (through ship time) support to CoASTS and BiOMaP activities was provided by: the JRC through the EOSS and COLORS institutional projects, the European Union through the MAST-III, EUROFLEETS and JERICO programs, the North Atlantic Treaty Organization (NATO) through the Science for Peace Program, the US National Aeronautics and Space Administration (NASA), the European Space Agency (ESA), the Romanian Space Agency (ROSA), the Institute of Oceanology of the Bulgarian Academy of Sciences, the Institute of Oceanology of the Polish Academy of Sciences, the Finnish Environment Institute, the Italian National Research Council, the Portuguese Hydrographic Institute, the Italian Hydrographic Institute, the Royal Belgian Institute of Natural Sciences, the Hellenic Centre for Marine Research, the Université du Littoral Côte d' Opale.
The contribution of Giuseppe Zibordi to the finalization of this work was supported by the National Aeronautics and Space Administration through the GESTAR-II program under award number 80NSSC22M0001, while the contribution of Jean-François Berthon was supported by DG DEFIS (the European Commission Directorate-General for Defence Industry and Space) and the Copernicus Programme.

12. References

Belward, A., Hartstra, J., Baruth, B., Beck, P., Carmona Moreno, C., Churchill, P., Craglia, M., Crandon, R., Ehrlich, D., Eva, H., Fortuny Guasch, J., Fullerton, K.T., Kemper, T., Kerdiles, H., Leo, O., Loudjani, P., Maenhout, G., Milenov, P., Pesaresi, M., Pinty, B., Zibordi, G. and Kreysa, J., A history of remote sensing at the JRC, Publications Office of the European Union, Luxembourg, 2022, ISBN 978-92-76-49465-2, JRC127849.

Berthon, J. F., Mélin, F., and Zibordi, G. (2008). Ocean colour remote sensing of the optically complex European seas. In *Remote sensing of the European seas* (pp. 35-52). Springer, Dordrecht.

Berthon, J-F., G. Zibordi, J.P. Doyle, S. Grossi, D. van der Linde, and C. Targa (2002). Coastal Atmosphere and Sea Time Series (CoASTS), Part 2: Data Analysis. *NASA Tech. Memo. 2002–206892, Vol. 20,* S.B. Hooker and E.R. Firestone, Eds., NASA Goddard Space Flight Center, Greenbelt, Maryland, 25 pp.

Doyle, J. P., and Zibordi, G. (2002). Optical propagation within a three-dimensional shadowed atmosphere–ocean field: application to large deployment structures. *Applied Optics*, *41*(21), 4283-4306.

https://doi.org/10.5194/essd-2024-240
Preprint. Discussion started: 26 June 2024

780 Doyle, J.P., S.B. Hooker, G. Zibordi, and D. van der Linde (2003). Validation of an In-Water,
781 Tower-Shading Correction Scheme. *NASA Tech. Memo. 2003–206892, Vol. 25,* S.B. Hooker
782 and E.R. Firestone, Eds., NASA Goddard Space Flight Center, Greenbelt, Maryland, 32 pp.
783 Ferrari, G. M., Dowell, M. D., Grossi, S., and Targa, C. (1996). Relationship between the optical
784 properties of chromophoric dissolved organic matter and total concentration of dissolved
785 organic carbon in the southern Baltic Sea region. *Marine Chemistry*, *55*(3-4), 299-316.
786 Ferrari, G. M., and Tassan, S. (1999). A method using chemical oxidation to remove light
787 absorption by phytoplankton pigments. *Journal of Phycology*, *35*(5), 1090-1098.
788 Gergely, M., and Zibordi, G. (2013). Assessment of AERONET-OC Lwn
789 uncertainties. *Metrologia*, *51*(1), 40.
790 Harris, R. L. (1999). *Information graphics: A comprehensive illustrated reference*. Oxford
791 University Press, USA, 448 pp.
792 Hooker S. B., Thomas C. S., Van Heukelem L., Russ M.E., Ras J., Claustre H., Clementson L.,
793 Canuti E., Berthon J.-F., Perl J. and Normandeau C. (2010). The fourth SeaWiFS HPLC
794 analysis round-Robin experiment (SeaHARRE-4). NASA. Technical Memorandum −2010–
795 215857. NASA Goddard Space Flight Center, Greenbelt, Maryland, 75 pp.
796 IOCCG (2000). Remote Sensing of Ocean Colour in Coastal, and Other Optically-Complex,
797 Waters. Sathyendranath, S. (ed.), *Reports of the International Ocean-Colour Coordinating*
798 *Group*, No. 3, IOCCG, Dartmouth, Canada.
799 IOCCG (2019). IOCCG Ocean optics and biogeochemistry protocols for satellite ocean colour
800 sensor validation. *IOCCG Protocols Series*, No.3, IOCCG, Dartmouth, Canada.
801 Jeffrey, S.W., R.F.C. Mantoura, and S.W. Wright (Eds.), 1997. *Phytoplankton Pigments in*
802 *Oceanography: Guidelines to Modern Methods.* UNESCO Publishing, Paris, 661 pp.
803 Maffione, R. A., and Dana, D. R. (1997). Instruments and methods for measuring the backward-
804 scattering coefficient of ocean waters. *Applied Optics*, *36*(24), 6057-6067.
805 Morel, A. (1974). Optical properties of pure water and pure seawater. *Optical aspects of*
806 *oceanography*.
807 Morel, A., Antoine, D., and Gentili, B. (2002). Bidirectional reflectance of oceanic waters:
808 accounting for Raman emission and varying particle scattering phase function. *Applied*
809 *Optics*, *41*(30), 6289-6306.
810 Mueller, J.L.,and R.W. Austin (1995). Ocean Optics Protocols for Sea-WiFS Validation,
811 Revision 1. *NASA Tech. Memo. 104566, Vol. 25,* S.B. Hooker and E.R. Firestone, Eds.,
812 NASA Goddard Space Flight Center, Greenbelt, Maryland, 67 pp.
813 Pérez, G. L., Galí, M., Royer, S. J., Sarmento, H., Gasol, J. M., Marrasé, C., and Simó, R.
814 (2016). Bio-optical characterization of offshore NW Mediterranean waters: CDOM
815 contribution to the absorption budget and diffuse attenuation of downwelling irradiance. *Deep*
816 *Sea Res. Part I Oceanogr.*, *114*, 111-127.
817 Stramski, D., and Kiefer, D. A. (1991). Light scattering by microorganisms in the open
818 ocean. *Progress in Oceanography*, *28*(4), 343-383.
819 Strickland, J.D.H., and T.R. Parsons, 1972: A practical handbook of sea water analysis. *Fish.*
820 *Res. Board. Canada,* 310 pp.
821 Tassan, S., and Ferrari, G. M. (1995). An alternative approach to absorption measurements of
822 aquatic particles retained on filters. *Limnology and oceanography*, *40*(8), 1358-1368.
823 Tassan, S., Ferrari, G. M., Bricaud, A., and Babin, M. (2000). Variability of the amplification
824 factor of light absorption by filter-retained aquatic particles in the coastal
825 environment. *Journal of Plankton Research*, *22*(4), 659-668.

https://doi.org/10.5194/essd-2024-240
Preprint. Discussion started: 26 June 2024

826 Thuillier, G., Hersé, M., Foujols, T., Peetermans, W., Gillotay, D., Simon, P. C., and Mandel, H.
827 (2003). The solar spectral irradiance from 200 to 2400 nm as measured by the SOLSPEC
828 spectrometer from the ATLAS and EURECA missions. *Solar Physics*, *214*(1), 1-22.
829 Twardowski, M. S., Boss, E., Macdonald, J. B., Pegau, W. S., Barnard, A. H., and Zaneveld, J.
830 R. V. (2001). A model for estimating bulk refractive index from the optical backscattering
831 ratio and the implications for understanding particle composition in case I and case II
832 waters. *Journal of Geophysical Research: Oceans*, *106*(C7), 14129-14142.
833 Van der Linde, D. (1998). Protocol for total suspended matter estimate. *JRC Technical Note I-*
834 *98-182*, Joint Research Centre of the European Commission, Ispra, Italy, 15 pp.
835 Van Heukelem, L., and Thomas, C. S. (2001). Computer-assisted high-performance liquid
836 chromatography method development with applications to the isolation and analysis of
837 phytoplankton pigments. *Journal of Chromatography A*, *910*(1), 31-49.
838 Zaneveld, J. R. V., Kitchen, J. C., Bricaud, A., and Moore, C. C. (1992, December). Analysis of
839 in-situ spectral absorption meter data. In *Ocean Optics XI* (Vol. 1750, pp. 187-200). SPIE.
840 Werdell, P. J., and Bailey, S. W. (2005). An improved in-situ bio-optical data set for ocean color
841 algorithm development and satellite data product validation. *Remote Sensing of*
842 *Environment*, *98*(1), 122-140.
843 Whitmire, A. L., Boss, E., Cowles, T. J., and Pegau, W. S. (2007). Spectral variability of the
844 particulate backscattering ratio. *Optics Express*, *15*(11), 7019-7031.
845 World Meteorological Organization, 1983: *Guide to the Meteorological Instruments and*
846 *Methods of Observation,* WMO–N.8, 517 pp.
847 Zhang, X., Stramski, D., Reynolds, R. A., and Blocker, E. R. (2019). Light scattering by pure
848 water and seawater: the depolarization ratio and its variation with salinity. *Applied*
849 *Optics*, *58*(4), 991-1004.
850 Zibordi, G. (2006). Immersion factor of in-water radiance sensors: assessment for a class of
851 radiometers. *Journal of Atmospheric and Oceanic Technology*, *23*(2), 302-313.
852 Zibordi, G., and Berthon, J-F. (2024). Coastal Atmosphere & Sea Time Series (CoASTS) and the
853 Bio-Optical mapping of Marine optical Properties (BiOMaP): the near-surface marine bio-
854 optical data set. Accessible at: https://doi. pangaea.de/10.1594/PANGAEA.968716.
855 Zibordi, G., J-F. Berthon, J.P. Doyle, S. Grossi, D. van der Linde, C. Targa, and L. Alberotanza
856 (2002). Coastal Atmosphere and Sea Time Series (CoASTS), Part 1: A Tower-Based Long-
857 Term Measurement Program. *NASA Tech. Memo. 2002–206892, Vol. 19,* S.B. Hooker and
858 E.R. Firestone, Eds., NASA Goddard Space Flight Center, Greenbelt, Maryland, 29 pp.
859 Zibordi, G., Berthon, J. F., Mélin, F., and D'Alimonte, D. (2011). Cross-site consistent in situ
860 measurements for satellite ocean color applications: The BiOMaP radiometric dataset. *Remote*
861 *Sensing of Environment*, *115*(8), 2104-2115.
862 Zibordi, G., and Bulgarelli, B. (2007). Effects of cosine error in irradiance measurements from
863 field ocean color radiometers. *Applied Optics*, *46*(22), 5529-5538.
864 Zibordi, G., Doyle, J. P., and Hooker, S. B. (1999). Offshore tower shading effects on in-water
865 optical measurements. *Journal of Atmospheric and Oceanic Technology*, *16*(11), 1767-1779.
866 Zibordi, G., Holben, B. N., Talone, M., D'Alimonte, D., Slutsker, I., Giles, D. M., & Sorokin, M.
867 G. (2021). Advances in the ocean color component of the aerosol robotic network
868 (AERONET-OC). *Journal of Atmospheric and Oceanic Technology*, *38*(4), 725-746.
869 Zibordi, G., Hooker, S. B., Mueller, J., and Lazin, G. (2004). Characterization of the immersion
870 factor for a series of in-water optical radiometers. *Journal of Atmospheric and Oceanic*
871 *Technology*, *21*(3), 501-514.

https://doi.org/10.5194/essd-2024-240
Preprint. Discussion started: 26 June 2024

872 Zibordi, G., and Voss, K. J. (2010). Field radiometry and ocean color remote sensing.
873 In *Oceanography from space* (pp. 307-334). Springer, Dordrecht.
874
875

https://doi.org/10.5194/essd-2024-240
Preprint. Discussion started: 26 June 2024

Appendix A: Acronyms

AERONET-OC	Ocean Color component of the Aerosol Robotic Network
BiOMaP	Bio-Optical mapping of Marine Properties
CDOM	Colored Dissolved Organic Matter
CoASTS	Coastal-Atmosphere and Sea Time-Series
HPLC	High-Pressure Liquid Chromatography
JRC	Joint Research Center
NASA	National Aeronautics and Space Administration
NIST	National Institute of Standards and Technology
NPL	National Physical Laboratory
SeaWiFS	Sea-viewing Wide Field-of-view Sensor
WiSPER	Wire-Stabilized Profiling Environmental Radiometer